Real-Time Observation of the Buildup of Soliton Molecules

Xueming Liu,[1,2,*] Xiankun Yao,[1] and Yudong Cui[1]
[1]State Key Laboratory of Modern Optical Instrumentation, College of Optical Science and Engineering, Zhejiang University, Hangzhou 310027, China
[2]State Key Laboratory of Transient Optics and Photonics, Xi'an Institute of Optics and Precision Mechanics, Chinese Academy of Sciences, Xi'an 710119, China

(Received 13 February 2018; published 12 July 2018)

Real-time spectroscopy access to ultrafast fiber lasers opens new opportunities for exploring complex soliton interaction dynamics. Here, we have reported the first observation, to the best of our knowledge, of the entire buildup process of soliton molecules (SMs) in a mode-locked laser. We have observed that the birth dynamics of a stable SM experiences five different stages, i.e., the raised relaxation oscillation (RO) stage, beating dynamics stage, transient single pulse stage, transient bound state, and finally the stable bound state. We have discovered that the evolution of pulses in the raised RO stage follows a law that only the strongest one can ultimately survive and, meanwhile, the pulses periodically appear at the same temporal positions for all lasing spikes during the same RO stage (named as memory ability) but they lose such ability between different RO stages. Moreover, we have found that the buildup dynamics of SMs is quite sensitive to both the polarization state of intracavity light and the fluctuation of pump power. These results provide new perspectives into the ultrafast transient process in mode-locked lasers and the dynamics of complex nonlinear systems.

DOI: 10.1103/PhysRevLett.121.023905

Dispersion is responsible for pulse broadening or compression that is dependent on the dispersion value [1–3]. Resulting from an elegant balance between dispersion and nonlinearity [3–6], however, the optical soliton has remarkable robustness over long-distance propagation. With a particlelike nature, the solitons exhibit profound nonlinear optical dynamics and excitation ubiquitous in many fields of physics [7–9], including fluids [10], plasmas [11], fibers [12], optical systems [13], complex networks [14], and Bose-Einstein condensates [15]. The mode-locked fiber laser constitutes an ideal test bed for investigating ultrashort pulse dynamics [16], where such pulses arise from the dynamical balance among nonlinearity, dispersion, and environmental energy exchange and then are referred to as dissipative solitons [7,17]. As several solitons coexist in a laser cavity, they can constitute the bound state, which is frequently referred to as the soliton molecule (SM) [1,8,18–21].

From the 1990s, the starting dynamics of mode-locked lasers had been reported experimentally and theoretically [22–24], yet the spectral dynamics during the buildup of pulse lasers has not been measured directly [1]. Recently, the dynamic behavior of mode-locked lasers has been investigated via the time-stretch dispersive Fourier transform (TS DFT) technique [25], in which the spectral information is mapped into the time domain [1,26,27]. This new technique opens new opportunities for exploring SM dynamics and then real-time observations of internal motion and the complex interaction dynamics of SMs in mode-locked lasers have been demonstrated [1,3]. Furthermore, transient coherent multisoliton states have been observed experimentally [17], where the short-lived SMs grow from noise and rapidly decay. However, the entire buildup process of stable long-lived SMs has not been discovered so far. Here, we demonstrate the first direct observation of the entire buildup process of stable SMs in a mode-locked fiber laser by means of the TS DFT technique. Our measurements reveal very complicated dynamics in the birth of SMs, e.g., the raised RO stage, beating behavior, Kelly sideband, spectrum induced by four-wave mixing (FWM), transient single soliton, and transient bound state.

Figure 1 illustrates the experimental setup. The laser system consists of a carbon nanotube saturable absorber (CNT SA), a segment of erbium-doped fiber (EDF), a polarization controller (PC), some single-mode fiber (SMF) pigtails, and a polarization-independent hybrid combiner of a wavelength division multiplexer, a tap coupler, and an isolator (WTI). The gain medium is a 3.5-m-long EDF with 6 dB/m peak absorption at 980 nm, pumped by a laser diode (LD). The CNT film acts as a modelocker to initiate the soliton operation. The PC and optical chopper are used to optimize the mode-locking performance and control the pump power, respectively. The dispersions of SMF and EDF are -22 and 11.6 ps^2/km at 1.55 μm, respectively, resulting in a net cavity dispersion of -0.06 ps^2. The total cavity length ~7.8 m entails a fundamental repetition rate of 26.3 MHz. The time-averaged spectral and real-time

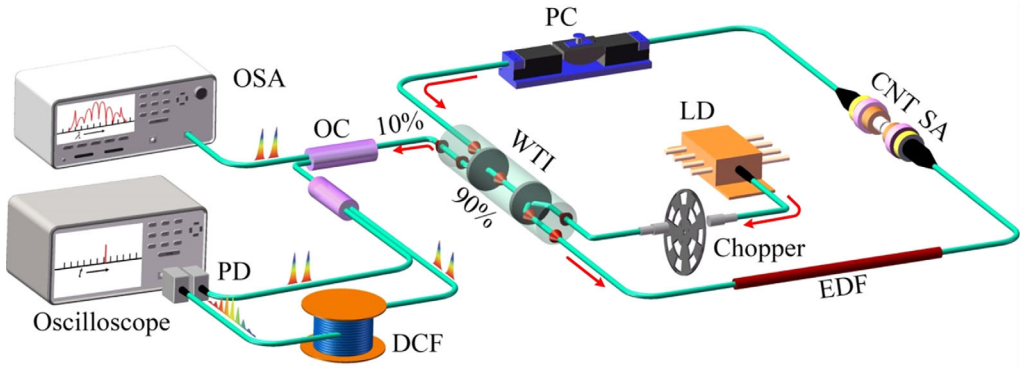

FIG. 1. Schematic diagram of the experimental setup for the mode-locked laser.

temporal detections are recorded with an optical spectrum analyzer (OSA) and a high-speed real-time oscilloscope (20 Gsamples/s sampling rate) together with a 25-GHz-bandwidth photodetector (PD), respectively. The DFT is implemented by temporally stretching the solitons in a 5-km-long dispersion-compensating fiber (DCF) with dispersion of about -160 ps/(nm km).

The mode-locked laser here emits the continuous wave, single soliton, and SMs at the pump power of ~10, ~16, and ~20 mW, respectively. Figures 2(a) and 2(b) show the recorded results over the entire buildup process of SMs in a mode-locked laser with and without the TS DFT technique, respectively. The recorded time series are segmented with respect to the round-trip time and then the buildup dynamics of solitons can be depicted by the round-trip time and the round-trip number. The y and x axes depict the time within a single round-trip (i.e., from 0 to ~38 ns) and the dynamics across consecutive round-trips, respectively. For the convenience of reference, we set the beginning time of the single-pulse mode-locking state as the zero round-trip number. The red curves in the insets of Figs. 2(a) and 2(b) denote the cross sections at the round-trip numbers of -570 and -590, respectively. The blue curves in the insets of Figs. 2(a) and 2(b) represent the cross sections at the intracavity time of 34.5 ns. An enlargement of RO stage and the corresponding cross sections in Fig. 2(a) are shown in Figs. S1(a)–S1(c) in the Supplemental Material [28].

Figure 2 demonstrates that a raised RO stage with six spikes occurs prior to the zero round-trip number and then the beating behavior, Kelly sidebands, and transient bound state appear before the stable SMs. The direct measurement only exhibits the information of solitons in the temporal domain, as shown in Fig. 2(b). A movie illustrates the experimental real-time observation in detail (see the Supplemental Material movie at Ref. [29]). Note that, in Figs. 2(a) and 2(b), the difference of the RO stage with and without the TS DFT technique originates from the resolution of the oscilloscope. After using the TS DFT technique, the picosecond or subpicosecond pulses are broadened to subnanosecond pulses [see Fig. S2(b) in the Supplemental Material [28] for details].

Figure 2(a) shows that, after the zero round-trip number, the oscilloscope records the spectral characterization of SMs. For example, Kelly sidebands appear at the wavelengths of about 1547 and 1578 nm, the spectra induced by

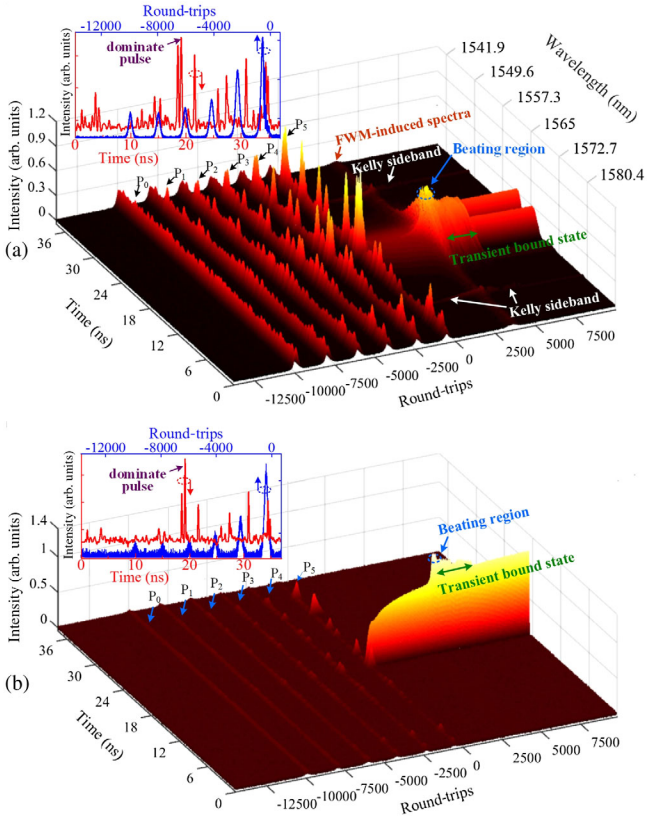

FIG. 2. Experimental real-time characterization of the entire buildup process of a SM in a mode-locked laser (a) with and (b) without the TS DFT technique, respectively. The intensity profile evolves along with the round-trip time (y axis) and the round-trip number (x axis). Insets in (a),(b) denote the cross sections at the -570 and -590 round-trip numbers (red curve) and at the time (blue curve) of 34.5 ns, respectively. Indications for P_0 to P_5 represent a pulse appearing on six spikes at the time of 34.5 ns. An enlargement of the raised RO stage in (a) is shown in Fig. S1 in the Supplemental Material [28].

FWM occur near 3500 round-trip, and the spectral modulation arises in the bound-state stage. See the Supplemental Material [30] for a full animation. All of these features cannot be observed in the direct measurement (see the Supplemental Material [29]). In contrast, prior to the zero round-trip number, the oscilloscope records the temporal information of SMs. A detailed description and an analysis for resolving the spectral and temporal information are given in the Supplemental Material [28]. The existence of a RO stage is a typical characteristics of the transient behavior of lasers [2,31,32]. Multiple pulses coexist in the laser cavity during this stage, where a typical example is shown in the inset of Fig. 2(a) (see the red curve) or Fig. S1(c) in the Supplemental Material [28]. The experimental observation demonstrates that multiple subnanosecond pulses appear in the RO stage but only one dominant pulse [see the insets of Figs. 2(a) and 2(b)] gradually evolves into the stationary mode-locking soliton. As a result, only the strongest pulse can survive ultimately and the others die.

The experimental results exhibit an interesting phenomenon; i.e., during the RO stage, the pulses are able to reappear at the same temporal positions for all lasing spikes. For instance, a pulse is observed at a fixed intracavity time of 34.5 ns for all six lasing spikes (see P_0 to P_5 in Fig. 2). Note that a fixed time in the y axis corresponds to a certain position of the cavity for each round-trip. The evolution of this pulse at the intracavity time of 34.5 ns over consecutive round-trips is shown in the insets of Fig. 2 (see the blue curves) or Fig. S1(b) in the Supplemental Material [28]. Although this pulse disappears at the round-trips from about −9500 to −8400, −7500 to −6500, −5500 to −4600, −3500 to −2700, and −1800 to −1100, it reappears at the same relative position in the laser cavity when it revives. Therefore, it seems that the pulses are able to "remember" some properties before their reappearance. This "memory ability" is a notable feature during the RO stage of mode-locked fiber lasers.

Using the TS DFT technique, we have recorded the shot-by-shot spectral information of the laser evolving [see Fig. 2(a)]. To reveal the formation and evolution of SMs, the planform of Fig. 2(a) is redrawn in Fig. 3. Figure 3(a) exhibits the experimental observations in the real-time series of interferograms, tracking the entire formation process of a stable SM. Figures 3(b) and 3(c) are enlargements of the A and B regions in Fig. 3(a), respectively. Figure 3(a) demonstrates that, after the RO stage, the soliton evolution of the mode-locked laser experiences different stages such as the transient single pulse, transient bound state, and finally the stable SM. An obvious beating behavior is observed between the RO stage and the transient single pulse stage, as shown in the A region of Fig. 3(a) or its expanded view [see Fig. 3(b)]. Clear Kelly sidebands appear in the transient single-pulse stage. The transient single pulse evolves to the transient bound state

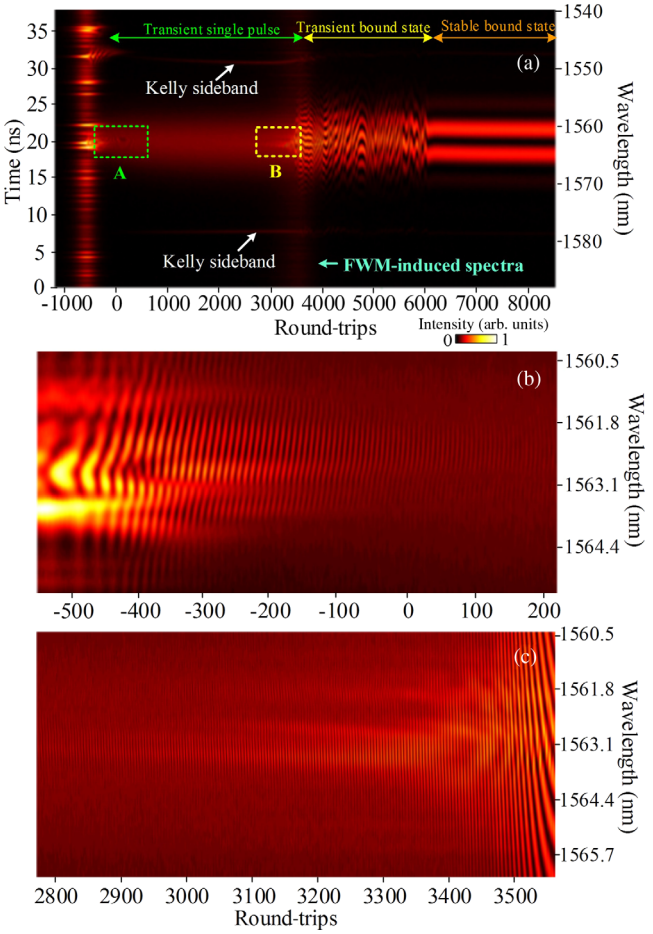

FIG. 3. Formation and evolution of a SM with beating dynamics. (a) Experimental real-time interferograms during the formation and evolution of SM. A full animation is shown in movie of the Supplemental Material [30]. (b),(c) Close-ups of the data from the A and B regions of (a), revealing the interference pattern for the beating dynamics.

after another beating process, as shown in Fig. 3(c) [an expanded view of the B region in Fig. 3(a)]. Figures 3(b) and 3(c) show that both of the two beating dynamics last over ∼800 round-trips. The full animation is demonstrated in the movie of the Supplemental Material [30]. During the round-trips from ∼3200 to 3800, as shown in Fig. 3(a), the laser spectra are slightly broadened by the spontaneous and multiple FWM effect [33,34].

Via the second beating process, one single soliton is broken into two. In succession, the transient bound state starts where two newly generated solitons interact intensively. The Fourier transform of each single-shot spectrum corresponds to the field autocorrelation of the momentary bound-state solitons [1], tracing the separation between the two solitons, as shown in Fig. 4(a). The real-time data illustrate the complex temporal evolution; e.g., two solitons arise from a single soliton near the round-trip of 3500 and the stable bound state appears after the round-trip of ∼6000 (see also the Supplemental Material [30]). Figure 4(b)

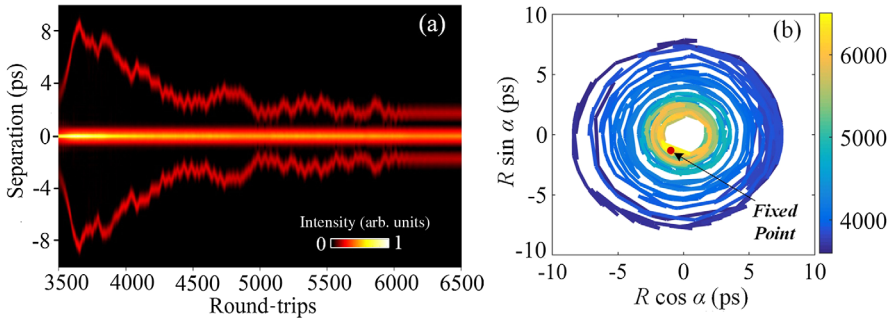

FIG. 4. (a) Field autocorrelation of each single-shot spectrum, exhibiting the separation between two solitons during the transient bound-state region. (b) Dynamics of the SM formation mapped into the interaction plane from about 3600 to 6500 round-trips.

shows the dynamics of the SM formation mapped into the interaction plane from about 3600 to 6500 round-trips. In Fig. 4(b), the angle (α) represents the relative phase between the two solitons and the radius (R) corresponds to the separation between them. The achievement for α is shown in the Supplemental Material [28]. Prior to the establishment of the stable bound state, the trajectory illustrates the evolution of the two solitons over periodic metastable soliton separations. Finally, the system reaches a fixed point with a locked relative phase, as shown in Fig. 4(b), and then two solitons form a SM settled at a constant binding separation together with a fixed phase relationship.

Figures 5(a) and 5(b) illustrate the spectra of the laser pulses measured by the OSA and the real-time TS DFT technique, respectively. Two curves in Fig. 5(a) demonstrate the same data with a linear or logarithmic scale. Figure 5(b) exhibits the last frame in the real-time series shown in Fig. 2(a). The experimental observations show that the real-time records have evident Kelly sidebands, which are typical characteristics of solitons in the presence of periodic amplification [35–37]. The real-time single-shot spectra measured by the TS DFT technique agree quite well with the time-averaged optical spectra measured by the OSA, highlighting the mapping relationship linked by the dispersion [38]. Therefore, the TS DFT technique can accurately map the spectral information of SMs [see Fig. 5(a)] into the temporal domain [see Fig. 5(b)].

For simplicity, the specific mapping relation can be expressed as [38,39]

$$\Delta t = |D| L \Delta\lambda, \tag{1}$$

where $\Delta\lambda$ is the bandwidth of the optical spectrum, Δt is the time spacing into which the optical spectrum is mapped, and D and L are the dispersion parameter and length of DCF, respectively. Since D is about -160 ps/(nm km) and L is 5 km in our experiments, the relation between the time spacing and the wavelength can be expressed as $\Delta t = 0.8\ \text{ns/nm} \times \Delta\lambda$. An example is that $\Delta t_1 = 12.6$ ns for $\Delta\lambda_1 = 15.8$ nm, where $\Delta\lambda_1$ and Δt_1 are the time spacing and spectral bandwidth from the first Kelly sideband to the central wavelength and central time, respectively, as shown in Fig. 5. Obviously, the experimental results show excellent agreement with the theoretical estimations using the equation above.

The RO stage is the general characterization of the transient behavior of lasers [2,31]. When the modelocker (i.e., CNT SA) is excluded from the experiment setup, the experimental results demonstrate that the laser starts at a RO stage with a damped behavior (see Fig. 6), rather than a raised behavior (see Fig. 2). Specifically, the laser without a modelocker emits a uniform optical wave distributed throughout the laser cavity (see Fig. 6), which is quite different from the mode-locked laser where multiple pulses are initiated at this stage [see Figs. 2(a) and 7(b)].

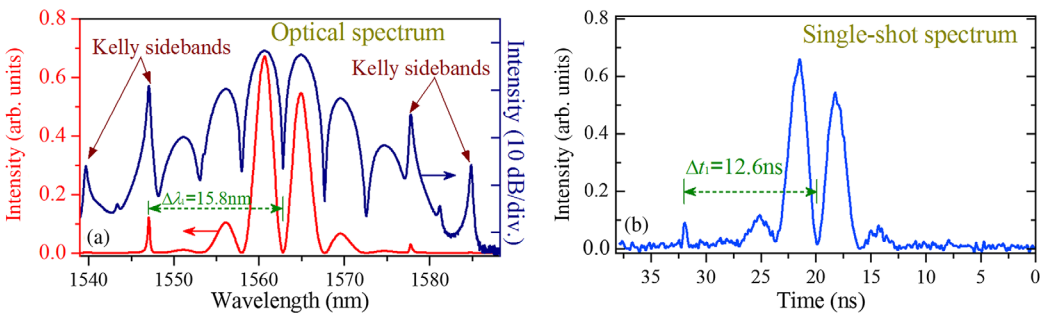

FIG. 5. (a) Optical spectra of SM measured by OSA. (b) Exemplary single-shot spectrum, corresponding to the last frame in Fig. 2(a).

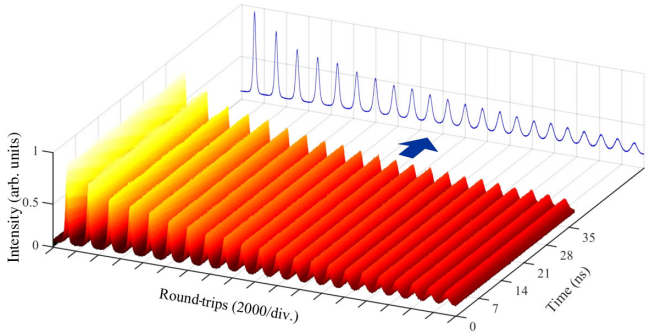

FIG. 6. RO stage of lasers without the modelocker. The projection on the round-trip intensity plane shows the intensity profile along with the round-trips.

In experiments, we have observed that the buildup process of dissipative solitons is quite sensitive to external perturbations such as the change of the light polarization state and the fluctuation of the pump power. Figure 7(a) demonstrates the buildup process of SMs in a laser mode-locked by the nonlinear polarization rotation technique. Because of the perturbation of the light polarization state, before the stable SM formation this laser experiences a complex transient process lasting over 2.3×10^5 round-trips, which is more than 23 times longer than that of the CNT-based mode-locked laser (see Fig. 2). Similar works were reported in Refs. [17,40]. The laser mode-locked by CNT SA is insensitive to the polarization change

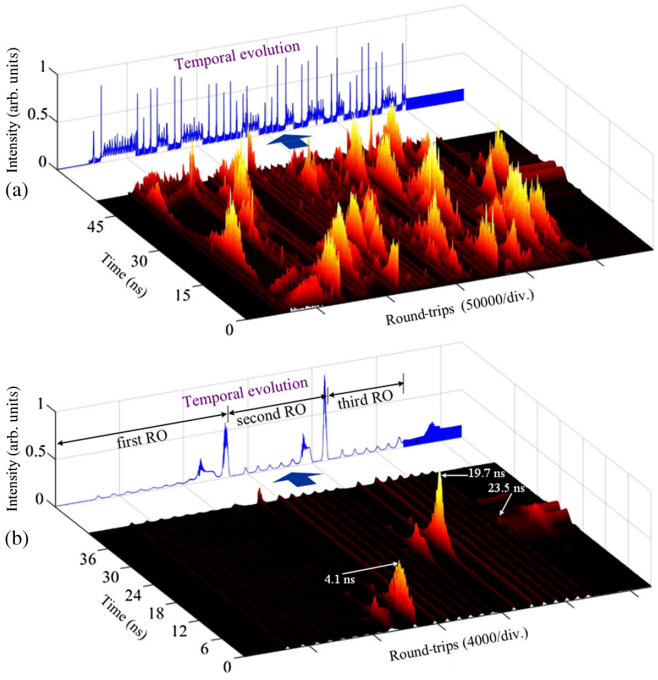

FIG. 7. Buildup process of SMs in lasers mode-locked by (a) the nonlinear polarization rotation technique and (b) CNT SA with a fluctuating pump power. The projection shows the temporal evolution along with the round-trips.

[19,36,41], yet the fluctuation of pump power can influence the birth of SMs. Figure 7(b) demonstrates a typical result where there exist three RO stages rather than only the one RO stage shown in Fig. 2. The pulses appear at the same temporal positions for all spikes in each RO stage, yet they occur on different positions between different RO stages. For instance, the strongest pulse appears at the temporal positions of about 4.1, 19.7, and 23.5 ns for the first, second, and third RO stages, respectively, as shown in Fig. 7(b). Therefore, the pulses only have the memory ability at the same RO stage but lose such ability between different RO stages. In this Letter, the influence of polarization change in the laser cavity has been overcome effectively by optimizing the CNT SA design and the laser system and, meanwhile, the fluctuation of pump power has also been decreased evidently. The fluctuations of pump power for Figs. 2 and 7(b) are shown in Figs. S5(a) and S5(b) in the Supplemental Material [28], respectively. As a result, the entire buildup process of SMs in mode-locked lasers is observed by using the emerging TS DFT technique.

In summary, we have experimentally demonstrated the evidence that the external perturbations (e.g., the change of the light polarization state and the fluctuation of pump power) can seriously influence the buildup process and dynamics of SMs. By decreasing such perturbations and optimizing the modelocker and the laser system, we have successfully tracked the formation and evolution of SMs in the cavity of mode-locked lasers using the TS DFT technique. Therefore, we have experimentally observed the real-time dynamics of the entire buildup process of stable SMs for the first time to our best knowledge. These observations show that the entire buildup process of SMs usually experiences five different stages, i.e., the raised RO stage, two times of the spectral beating dynamics stage, transient single pulse stage, transient bound state, and finally stable bound state. The mode-locked laser (i.e., with a modelocker) undergoes the raised RO stage where multiple pulses occur; however, the laser without a modelocker experiences the damped RO stage where no pulse appears. We discover two interesting phenomena in mode-locked lasers; i.e., the pulses in the raised RO stage evolve with the rule of the survival of the strongest and they have the memory ability at the same RO stage [see Fig. 2(a)] but lose such ability between different RO stages [see Fig. 7(b)]. We believe that our results can provide some new perspectives into the ultrafast transient dynamics of mode-locked lasers and will bring useful insights into laser designs and applications.

We thank M. Pang, X. Han, G. Chen, W. Li, G. Wang, and Y. Zhang for fruitful discussions. This Letter was partially supported by the National Natural Science Foundation of China under Grants No. 61525505, No. 11774310, and No. 61705193 and by the Key Scientific and Technological Innovation Team Project in Shaanxi Province (2015KCT-06).

*Corresponding author.
liuxueming72@yahoo.com

[1] G. Herink, F. Kurtz, B. Jalali, D. R. Solli, and C. Ropers, Science **356**, 50 (2017).
[2] O. Svelto, *Principles of Lasers* (Springer, New York, 2010).
[3] K. Krupa, K. Nithyanandan, U. Andral, P. Tchofo-Dinda, and P. Grelu, Phys. Rev. Lett. **118**, 243901 (2017).
[4] G. Herink, B. Jalali, C. Ropers, and D. R. Solli, Nat. Photonics **10**, 321 (2016).
[5] M. Pang, W. He, X. Jiang, and P. S. J. Russell, Nat. Photonics **10**, 454 (2016).
[6] P. J. Ackerman and I. I. Smalyukh, Phys. Rev. X **7**, 011006 (2017).
[7] P. Grelu and N. Akhmediev, Nat. Photonics **6**, 84 (2012).
[8] M. Stratmann, T. Pagel, and F. Mitschke, Phys. Rev. Lett. **95**, 143902 (2005).
[9] A. Armaroli, C. Conti, and F. Biancalana, Optica **2**, 497 (2015).
[10] T. Dauxois and M. Peyrard, *Physics of Solitons* (Cambridge University, Cambridge, 2015).
[11] N. J. Zabusky and M. D. Kruskal, Phys. Rev. Lett. **15**, 240 (1965).
[12] L. G. Wright, D. N. Christodoulides, and F. W. Wise, Science **358**, 94 (2017).
[13] J. M. Dudley, F. Dias, M. Erkintalo, and G. Genty, Nat. Photonics **8**, 755 (2014); G. I. Stegeman and M. Segev, Science **286**, 1518 (1999).
[14] S. Strogatz, Nature (London) **410**, 268 (2001).
[15] J. Denschlag, J. Simsarian, D. Feder, C. W. Clark, L. Collins, J. Cubizolles, L. Deng, E. W. Hagley, K. Helmerson, and W. P. Reinhardt, Science **287**, 97 (2000).
[16] A. F. J. Runge, N. G. R. Broderick, and M. Erkintalo, Optica **2**, 36 (2015).
[17] P. Ryczkowski, M. Närhi, C. Billet, J. M. Merolla, G. Genty, and J. M. Dudley, Nat. Photonics **12**, 221 (2018).
[18] A. Hause and F. Mitschke, Phys. Rev. A **88**, 063843 (2013); K. Lakomy, R. Nath, and L. Santos, Phys. Rev. A **86**, 013610 (2012).
[19] X. Liu, X. Han, and X. Yao, Sci. Rep. **6**, 34414 (2016).
[20] A. Zavyalov, R. Iliew, O. Egorov, and F. Lederer, Phys. Rev. A **80**, 043829 (2009).
[21] Y. Wang, F. Leo, J. Fatome, M. Erkintalo, S. G. Murdoch, and S. Coen, Optica **4**, 855 (2017).
[22] J. Herrmann, Opt. Commun. **98**, 111 (1993).
[23] N. W. Pu, J. M. Shieh, Y. Lai, and C. L. Pan, Opt. Lett. **20**, 163 (1995).
[24] H. Li, D. G. Ouzounov, and F. W. Wise, Opt. Lett. **35**, 2403 (2010).
[25] K. Goda, K. K. Tsia, and B. Jalali, Nature (London) **458**, 1145 (2009).
[26] Y. Xu, X. Wei, Z. Ren, K. K. Y. Wong, and K. K. Tsia, Sci. Rep. **6**, 27937 (2016).
[27] A. Mahjoubfar, D. V. Churkin, S. Barland, N. Broderick, S. K. Turitsyn, and B. Jalali, Nat. Photonics **11**, 341 (2017).
[28] See Supplemental Material at http://link.aps.org/supplemental/10.1103/PhysRevLett.121.023905 for more detailed discussions.
[29] See Supplemental Material at http://link.aps.org/supplemental/10.1103/PhysRevLett.121.023905 for a movie showing the experimental real-time measurements from direct measurement (i.e., not using TS DFT) for the formation and evolution of soliton molecules.
[30] See Supplemental Material at http://link.aps.org/supplemental/10.1103/PhysRevLett.121.023905 for a movie showing the experimental real-time measurements from DCF (i.e., with the TS DFT technique) for the formation and evolution of soliton molecules.
[31] R. Dunsmuir, J. Electron. Control **10**, 453 (1961).
[32] I. Mozjerin, S. Ruschin, and A. A. Hardy, IEEE J. Quantum Electron. **46**, 158 (2010).
[33] S. Gao, C. Yang, X. Xiao, Y. Tian, Z. You, and G. Jin, Opt. Express **14**, 2873 (2006).
[34] X. Liu, Phys. Rev. A **77**, 043818 (2008).
[35] S. M. J. Kelly, Electron. Lett. **28**, 806 (1992).
[36] X. Liu, Y. Cui, D. Han, X. Yao, and Z. Sun, Sci. Rep. **5**, 9101 (2015).
[37] H. A. Haus and W. S. Wong, Rev. Mod. Phys. **68**, 423 (1996).
[38] K. Goda and B. Jalali, Nat. Photonics **7**, 102 (2013).
[39] K. Goda, D. R. Solli, K. K. Tsia, and B. Jalali, Phys. Rev. A **80**, 043821 (2009).
[40] X. Wei, B. Li, Y. Yu, C. Zhang, K. K. Tsia, and K. K. Y. Wong, Opt. Express **25**, 29098 (2017).
[41] A. G. Rozhin, Y. Sakakibara, and S. Namiki, Appl. Phys. Lett. **88**, 051118 (2006).